Available online at www.sciencedirect.com
SCIENCE DIRECT®
Journal of Non-Crystalline Solids 331 (2003) 145–156
JOURNAL OF NON-CRYSTALLINE SOLIDS
www.elsevier.com/locate/jnoncrysol

Isothermal sintering with concurrent crystallization of polydispersed soda–lime–silica glass beads

Miguel O. Prado *,[1], Catia Fredericci, Edgar D. Zanotto

Vitreous Materials Laboratory (LaMaV), Department of Materials Engineering (DEMa), Federal University of São Carlos (UFSCar), CEP 13.565-905 São Carlos, SP, Brazil

Received 28 April 2003

Abstract

The *Clusters* model, previously developed to describe the viscous sintering kinetics of polydispersed powders undergoing simultaneous surface crystallization, was tested in isothermal sintering experiments of devitrifying spherical glass particle compacts. The experiments were conducted at different temperatures to vary the relative kinetics of sintering and crystallization. The viscosity, glass–vapor surface energy, particle size distribution, average number of neighbors around each particle, particle to sample size ratio, and the effect of pre-existing surface crystals on the sintering kinetics were determined and taken into account in the calculations. The model describes the experimental sintering kinetics for a series of temperatures for two different size distributions and predicts the saturation of densification due to pre-existing surface crystals and surface crystallization. The calculations and experimental results confirmed that higher temperatures benefit sintering over crystallization.

1. Introduction

An alternative route to traditional glass–ceramic technology is the sintering and crystallization of glass powders. Through this process, it is possible to manufacture metal–ceramic or ceramic–ceramic composites, substrates, fiber reinforced glass–ceramics and dense or porous glass–ceramics [1]. However, many experiments are required to empirically establish the best conditions to obtain dense or porous bodies having controlled crystallinity. Based on the Frenkel (F) [2] and Mackenzie–Shuttleworth (MS) [3] models for sintering and the Johnson–Mehl–Avrami–Kolmogorov (JMAK) theory of crystallization [4], the *Clusters* model [5–7] was developed to compute the densification kinetics of complex systems undergoing sintering with concurrent crystallization. A strong motivating factor for this work, and of practical value, is that these phenomena can be simulated, thus reducing the number of experiments needed to reach optimum densification conditions.

The F and MS models, developed for monodispersed spherical particles and pores, describe only

* Corresponding author. Tel.: +54-2944 445 230; fax: +54-2944 445 299.
E-mail address: pradom@cab.cnea.gov.ar (M.O. Prado).
URL: http://www.nit.ufscar.br/lamav.
[1] On leave from the Comisión Nacional de Energía Atómica-Centro Atómico Bariloche, Av. Ezequiel Bustillo km 9.5, 8400 San Carlos de Bariloche (RN), Argentina.

0022-3093/$ - see front matter © 2003 Elsevier B.V. All rights reserved.
doi:10.1016/j.jnoncrysol.2003.08.076

the early and final steps of the sintering process, respectively. Recently, the Clusters model [5] was shown to describe the sintering kinetics of polydispersed glass particle compacts. This model assumes the clustering of equal sized particles, the formation of necks among particles in each cluster, the distribution of pore sizes and the simultaneous occurrence of the Frenkel and Mackenzie–Shuttleworth regions, a possibility that was pointed out earlier by Giess et al. [8].

In Ref. [5], the Clusters model was tested with *isothermal* sintering of an alumino-borosilicate glass that was stable against crystallization in the temperature range where sintering is measurable. In Ref. [6], the model was tested with *non-isothermal* sintering of the same glass and also using sintering data for cordierite glass, Ref. [9], which crystallizes easily. In these cases, irregularly shaped powders were used, introducing complicating factors such as the unknown 'shape factor' and non-uniform particle packing. In further tests [7], spherical glass particles with a known size distribution were used and for the first time, the effect of pre-existing surface crystals and the average number of neighbors around each particle were introduced into the calculations, having negligible crystallization during sintering. In Ref. [7], an effort was made to interpret the sample's porosity by comparing the calculated pore size distribution (by the Clusters model) with the measured one.

In the present work, a thorough study is made of the *competition* of sintering and crystallization of glass spheres with different size distributions at different temperatures. The main difference with Ref. [7] is that now, surface crystallization takes place during sintering.

2. Summary of the Clusters model

The Clusters model has been presented in other publications [5–7]; thus, we will review it but briefly here.

Based on the linear shrinkage $\Delta\mathbf{L}$, the original length of the sample $\mathbf{L}_0$, the temperature dependent viscosity $\eta(T)$, the glass–vapor surface energy γ, the compact's green density ρ_0, the glass density ρ_g and the sintering time t, the Frenkel equation of sintering is:

$$\frac{\mathrm{d}\left[\frac{\Delta L}{L_0}\right]}{\mathrm{d}t} = \frac{3\gamma k_s}{8\eta(T)r}, \tag{1}$$

where k_s is a shape factor ($k_s = 1$ for spherical particles), and r is the particle radius.

If shrinkage is isotropic, then

$$\rho = \frac{\rho_0}{\left[1 - \frac{\Delta L}{L_0}\right]^3}. \tag{2}$$

Using Eqs. (1) and (2) with $C = 3k_s\gamma/8r$, the sintering rate for an isothermal process can be written in terms of the relative densities:

$$\frac{\mathrm{d}\rho}{\mathrm{d}t} = 3 \cdot C\rho_0^{-\frac{1}{3}}\rho^{\frac{4}{3}}/\eta(T). \tag{3}$$

These equations are valid for the first 10% of linear shrinkage or $\rho_0 \sim 0.8$ when beginning from $\rho_0 \sim 0.6$.

In the final stages of sintering, when spherical pores are isolated in the glass matrix, the Mackenzie–Shuttleworth (MS) model gives the following relationships [10]:

$$\frac{\mathrm{d}\rho}{\mathrm{d}t} = \frac{3\gamma}{2a_0\eta(T)}(1-\rho) \tag{4a}$$

or,

$$\rho(t) = 1 - (1-\rho_0)\mathrm{e}^{\left(\frac{-3\gamma t}{2a_0\cdot\eta(T)}\right)}, \tag{4b}$$

$$\frac{\mathrm{d}\rho}{\mathrm{d}t} = (1-\rho_0)\frac{-3\gamma}{2a_0\eta(T)}\mathrm{e}^{\left(\frac{-3\gamma t}{2a_0\cdot\eta(T)}\right)}, \tag{4c}$$

where a_0 is the initial radius of the spherical pores. To eliminate the dependence of the densification rate on ρ, Eq. (4a) must first be integrated to obtain Eq. (4b), after which the resulting Eq. (4b) must be derived to obtain the densification rate (Eq. (4c)).

Eq. (4a) is presented in a simplified form that allows for a simple mathematical treatment [10]. At present, we approximate $(1-\rho)/a$ by $(1-\rho)/a_0$, where a is the time-dependent pore radius, which is assumed to shrink during sintering while the number of pores remains constant. Due to this approximation, Eq. (4a) slightly underestimates

the sintering rate. Thus, it takes longer than it should to achieve the calculated final density.

If there are p phases ($p = 1, 2, \ldots$) crystallizing on the particle surfaces, each one with a density of surface nucleation sites N_p and a growth velocity $U_p(T)$, the crystallized surface fraction, α_s, after a period t at a temperature T may be estimated by the classical JMAK equation [4]:

$$\alpha_s = 1 - e^{\left(-\pi \sum_p N_p U_p(T)^2 \cdot t^2\right)}. \tag{5}$$

Here, we have assumed the most typical case, i.e., heterogeneous nucleation of spherical crystals growing on the glass surface at a linear growth rate $U_p(T)$ from a fixed number of sites per unit area, N_p.

Müller et al. [11] *assumed* that (regardless of the sintering model) the densification rate should decrease proportionally to the vitreous surface fraction remaining after crystallization. Thus, in that case, the isothermal densification rate is

$$\frac{d\rho_c}{dt} = \frac{d\rho}{dt}(1 - \alpha_s), \tag{6}$$

where ρ_c is the relative density of a compact that partially devitrifies during sintering.

Inserting the appropriate expressions for $d\rho/dt$ (Eqs. (3) and (4c)) and α_s (Eq. 5) into Eq. (6), taking into account the packing factor, p_f, and the glassy surface fraction, x_f, after integrating, one gets Eqs. (7) and (8) for the Frenkel and Mackenzie–Shuttleworth cases, respectively. In the equations x_f stands for the initial vitreous surface fraction of the particles before the onset of sintering, this factor arises when the particle surfaces contain pre-existing crystals, i.e. $x_f = 1 - \alpha_s(0)$, and p_f stands for the average number of necks that each particle develops with its neighbors, see Ref. [7].

$$\rho_{c,F}(t) = \rho_0 + \frac{3 \cdot C \rho_0 x_f p_f}{\eta(T)} \int_0^t \left(1 - \frac{C}{\eta(T)} t'\right)^{-4} \times e^{-\pi N_s U(T)^2 t'^2} dt', \tag{7}$$

$$\rho_{c,MS}(t) = \rho_0 + (1 - \rho_0)\left(\frac{C' x_f}{\eta(T)}\right) \times \int_0^t e^{\left(\frac{-C' t'}{\eta(T)}\right)} e^{-\pi N_s U(T)^2 t'^2} dt', \tag{8}$$

where $C = \frac{3\gamma}{8r}$ and $C' = \frac{3\gamma}{2a_0}$.

When the particle surface is pristine, $x_f = 1$. The probability that a neck between particles is of the glass–glass type is x_f^2. Eq. (8) assumes that the pore surfaces are remainders of the original particle surfaces, containing inculsions, etc., thus x_f affects the MS kinetics.

With these equations and the appropriate physical parameters of the glass (particle size distribution, relative green density, surface tension, viscosity versus temperature, number of active surface sites and crystal growth rate versus temperature), densification kinetics can be predicted at any chosen temperature. Except for $U(T)$, which must be measured, the other parameters can be estimated from the glass composition (η, γ) or used as free simulation parameters (N_s, v_r, ρ_0).

The relative density $\rho(t)$ during isothermal sintering of a polydispersed powder compact having a volume fraction v_r of particles of radius r that does not undergo crystallization can be expressed as [5,6]

$$\rho(t) = \left(\sum_r [\rho_F(r,t) \cdot \theta_F(t_{0.8} - t)\xi_r + \rho_{MS}(r,t) \cdot \theta_{MS}(t - t_{0.8})] v_r \right) \Big/ \left(\sum_r [\theta_F(t_{0.8} - t)\xi_r + \theta_{MS}(t - t_{0.8})] v_r \right), \tag{9}$$

where ξ_r is the neck-forming ability of each particle, which can be calculated from the particle size distribution [5]. For each cluster, the transition from the Frenkel regime to the MS regime is made using the temperature step functions $\theta_F(t_{0.8} - t)$ and $\theta_{MS}(t - t_{0.8})$, whose values switch between 1 and 0 at $t = t_{0.8}$ when $\rho_F(r, t_{0.8}) = 0.8$ is reached. Thus, $\theta_F(t_{0.8} - t) = 1$ and $\theta_{MS}(t - t_{0.8}) = 0$ for $t < t_{0.8}$, and $\theta_F(t_{0.8} - t) = 0$ and $\theta_{MS}(t - t_{0.8}) = 1$ for $t > t_{0.8}$. Eq. (9) summarizes the relative density $\rho(r,t)$ of each particle size, r, as a function of time, t. The subscript F indicates sintering in the Frenkel stage (we assume, as in Ref. [5], that $\rho(r,t) < 0.8$ in the Frenkel stage), and subscript MS indicates Mackenzie–Shuttleworth stage.

If the particle size distribution is not large, as in the present case, then $\xi_r = 1$ and Eq. 9 can be written more simply:

$$\rho(t) = \sum_r [\rho_F(r,t) \cdot \theta_F(t_{0.8} - t) + \rho_{MS}(r,t) \cdot \theta_{MS}(t - t_{0.8})] v_r. \quad (10)$$

Polydispersed distributions undergoing isothermal sintering and concurrent crystallization can be treated by introducing Eqs. (7) and (8) into Eqs. (9) or (10), namely $\rho_F(r,t)$ is calculated from Eq. (7) and $\rho_{MS}(r,t)$ from Eq. (8).

3. Materials and methods

In this study, compacts of commercial soda-lime-silica glass beads were used because: (i) the sintering models used here are based on spherical particles, and (ii) soda-lime-silica glass is a complex system with various crystalline phases appearing during crystallization, thus rendering it a good material to test the performance of the Clusters model under real service conditions.

We used two different size distributions (D1 and D2) of soda-lime-silica glass spheres (Potters Industrial Ltd.) with the following composition: 72.5 SiO_2, 13.7 Na_2O, 9.8 CaO, 3.3 MgO, 0.4 Al_2O_3, 0.2 FeO/Fe_2O_3, 0.1 K_2O wt%. The beads are manufactured with recyclable float glasses.

Fig. 1 shows the measured size distributions of D1 and D2. A certain quantity of spherical particles was distributed on a flat plate and, with the help of a KS 2000 Imaging System, Version 3.0, coupled to a Zeiss Axioskop optical microscope, the size of about 300 particles was determined for each distribution.

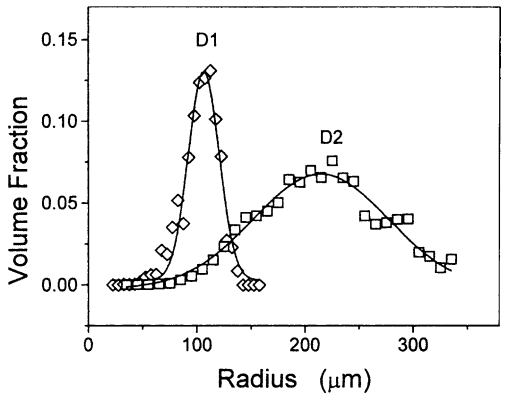

Fig. 1. Glass spheres size distributions D1 and D2.

The glass density for each type of distribution was measured by He picnometry. The calorimetric glass transition temperature, $T_g \sim 823$ K, was estimated by differential scanning calorimetry. The glass powder granulometry was <74 μm and the heating rate was 20 °C/min.

Approximately 60 g of glass spheres were melted in a platinum crucible at 1550 °C for 2 h. The liquid was poured onto a 2 cm × 3 cm cylindrical graphite mold. One glass slab was cut and its parallel faces were polished for low-temperature viscosity measurements (up to 820 °C) using the penetration method. Viscosity at high temperatures was determined by the rotating cylinder method in a Theta viscometer at a maximum temperature of 1600 °C. The temperature-viscosity curve was obtained by fitting a Vogel–Fulcher–Tammann equation $(\log \eta = A + B/(T - T_0))$ to the low and high viscosity data, and assuming that viscosity at the calorimetric glass transition temperature is 10^{12} Pa s.

A certain amount of glass spheres were treated at 680, 690, 700, 720 and 800 and 840 °C for different times in an electrical furnace having a thermal stability of ±2 °C. After a pre-determined time, the spheres were removed from the furnace and the crystals on their surfaces analyzed under an optical microscope. A surface region of low density of crystals was chosen and a digital image made from it. With the aid of the Imaging System KS 2000 3.0, the sizes of the selected crystals (those which were isolated from other crystals) were measured after sequential heat-treatments at the temperatures listed above. Crystal growth rates were obtained from these measurements.

After the crystal sizes had reached the limit of the optical microscope's range, the crystal growth rate was studied by both optical and electron microscopy. To this end, we investigated the heat-treated samples at low voltage in a field-emission gun FEG-SEM device, because this technique obviates the need for coating the sample, allowing the same sample to be treated for different lengths

of time without a coating interfering in the crystal growth rates. The U values obtained by the two techniques were found to be in close agreement.

The average number of crystals per unit area for each phase (N_p) was counted by scanning electron microscopy. The samples were heat-treated at 700 °C/5 h, 751 °C/45 min, 800 °C/40 min and 850 °C/40 min. These times and temperatures were chosen to render individual crystals and different morphologies distinguishable.

Spheres D1 or D2 were put in cylindrical aluminum crucibles with an internal volume of about 0.6 cm^3. The initial relative green density (ρ_0), was about 0.62 g/cm^3 for both distributions. The compacts were sintered in air, at temperatures of 655, 673, 710, and 751 °C for different times. After reaching the desired time (previously established by our algorithm), the samples were air-quenched to room temperature to preclude any additional sintering and crystallization on the cooling path. The sintered compact densities were determined by the Archimedes method, using mercury buoyancy.

We expected that larger particles sinter more slowly, allowing crystallization to overcome sintering. This effect was tested in sintering experiments, using distributions D1 and D2.

4. Results

4.1. Density, viscosity, surface energy and particle size distribution

At 298 K, the density values of (2.4622 ± 0.0005) g/cm^3 and (2.4735 ± 0.0005) g/cm^3 were found for D1 and D2, respectively. The soda-lime-silica glass used to produce the spheres has a true density of 2.51 g/cm^3, but the glass spheres contained a few bubbles, which decreased their density. These values were therefore used throughout this paper.

We found the following VFT parameters for the viscosity in Pa s: $A = -2.7$, $B = 4358.44$ K and $T_0 = 533$ K.

The glass–vapor surface energy, γ, is 0.325 J/m^2 [12], the only data taken from the literature and used in this paper. Fig. 1 shows both particle size distributions used here.

4.2. Glass beads surface

Since sintering and crystallization begin on the glass sphere's surface, these were analyzed by scanning electron microscopy (SEM). Several foreign particles on the glass beads surface are shown in Fig. 2 for a sphere taken from the D2 size distribution, in the as-received condition. Similar surface quality was observed in spheres from the D1 distribution. We hoped that these were nucleation sites that would induce partial crystallization, concurrently with sintering, allowing us to test the Cluster model under this arresting condition.

It is well-known that surface nucleation kinetics is governed by the presence of nucleation sites, such as dust particles, corners, edges and tips [13]. Pre-existing surface crystals prevent some sphere-sphere contacts from developing sintering necks since, at typical sintering temperatures, which are well below the melting point, crystalline particles cannot undergo viscous flow. The surface fraction affected by the inclusions observed and evaluated with optical microscopy is about 20%; however, our calculations indicated that 10% was an optimal value to account for the effect of these inclusions on the sintering kinetics. This mismatch between the surface affected by inclusions, as determined by electron microscopy, and the value obtained by fitting our model may be due to the fact that we could not determine the nature of these inclusions because of their small size and

Fig. 2. Scanning electron micrograph of a glass sphere surface, from the D2 size distribution. Width of the micrograph = 200 μm.

thickness. If some of the inclusions are glass relicts, with a viscosity similar to that of the particles, they will undergo viscous flow and will therefore not strongly affect the sintering kinetics.

4.3. Crystal growth rate (U) and numbers of crystals (N_s)

We measured the crystal growth rates for 4 crystalline phases: spherulites, needles, sticks and bipyramidal crystals. These were the predominant morphologies in the samples heat-treated in the range of 680–840 °C (Fig. 3(a)–(c)).

The procedure described in Section 3 was used for this purpose. Fig. 4(a) and (b) show SEM micrographs of the same sample heat-treated at a given temperature for different times. Fig. 5 shows the measured crystal growth rates.

Fig. 6 shows the density of crystal surface nucleation sites corresponding to the four morphologies at different temperatures. There is a large statistical scatter around each mean value for the

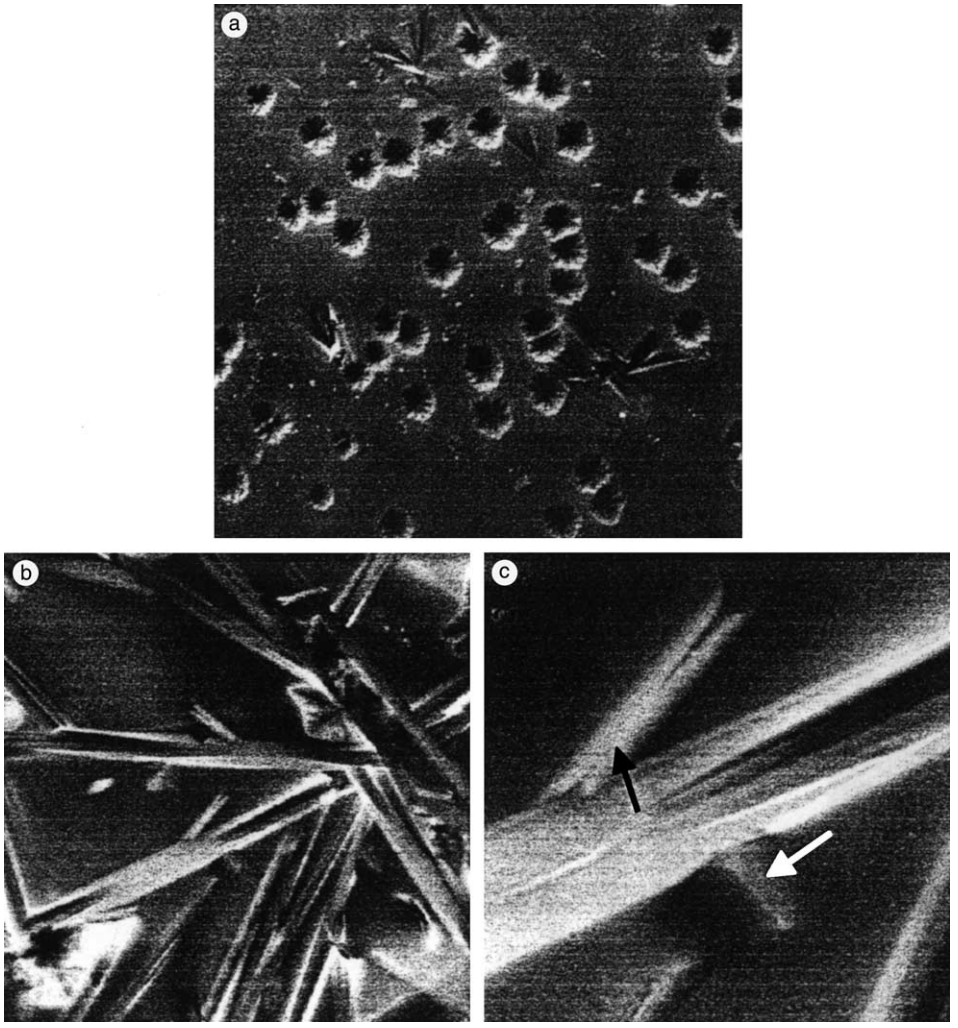

Fig. 3. SEM micrographs of a glass sphere surface heat-treated at: (a) 700 °C/5 h, spherulitic crystals are shown, (b) 840 °C/90 min and (c) the same sample as (a) but with a needle like crystal, it can be observed stick (black arrow) and bipyramidal crystals (white arrow). Width of the micrographs: (a) 150 μm, (b) 20 μm, (c) 7 μm.

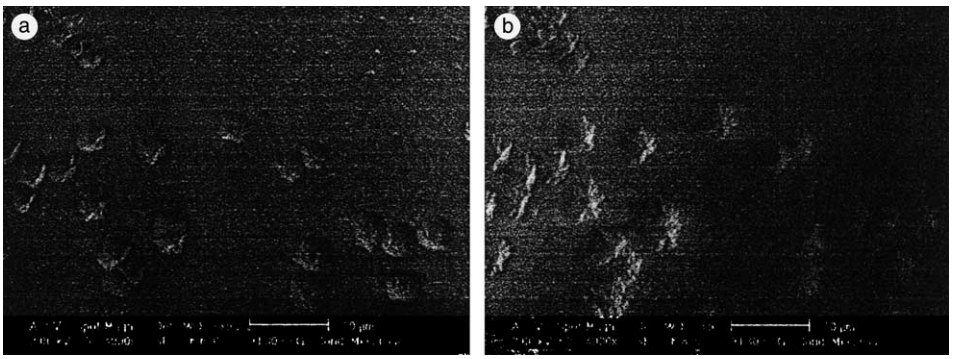

Fig. 4. FEG-scanning electron micrograph of the same sample heat-treated at 680 °C: (a) for 10 h and (b) for 12 h. Note that it is possible to identify the same crystal in each image.

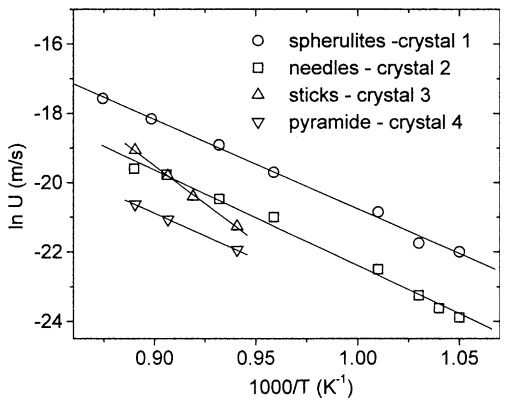

Fig. 5. Crystal growth rates of the four morphologies developed on the glass sphere surfaces during heat-treatment.

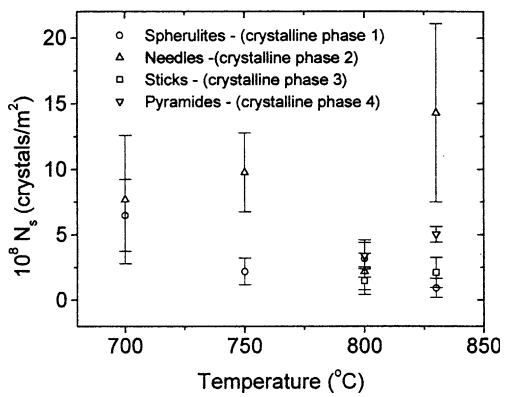

Fig. 6. Average number of crystals per m^2 on soda-lime-silica glass sphere surfaces after treatment at different times and temperatures: 700 °C/5 h, 751 °C/45 min, 800 °C/40 min and 850 °C /40 min.

all morphologies, which is typical for heterogeneous surface nucleation [13].

Table 1 summarizes the data for the four different crystalline phases found.

We refer to phases 1, 2, 3 and 4, since it was not possible to associate morphology to crystalline phase. However, the literature states that spherulitic (crystal 1) and needle-like crystals growing on soda-lime-silica glass (crystal 2) are cristobalite and devitrite, respectively. X-ray diffraction of samples heat-treated at 751 °C for 14 h and 900 °C for 6 h are presented in Fig. 7. The crystalline phases were identified as cristobalite, devitrite, β-wollastonite, quartz and diopside. Deubener et al. [14] identified pyramidal crystals as sodium metasilicate, but at the temperatures and times studied in this work we did not detect this crystalline phase. Further work is required to precisely associate the crystalline phases with morphology, although such determination is not essential to this work.

Most of the crystalline phases nucleated and grew from the particle surfaces. However, a few crystals nucleated on bubbles or heterogeneities in the bulk. It is also interesting to observe that the predominant crystalline phase changed with the annealing temperature.

4.4. Simulations and test of the model with two different size distributions

Using the data of Sections 4.1–4.3 and the model described in Section 2, we constructed

Table 1
Data about the main four crystalline phases appearing in the glass surface

Phase N	Morphology	Identified as	N_s (m^{-2})	$U(T)$ ($m\,s^{-1}$)
1	Spherulites	Cristobalite	3.0×10^9	$e^{(-27594/T+5.20)}$
2	Needles	Devitrite	1.1×10^9	$e^{(-27657/T+6.93)}$
3	Sticks	Not identified	1.8×10^8	$e^{(-43910/T+20.01)}$
4	Bipyramidal	Not identified	1.8×10^8	$e^{(-26222/T+2.17)}$

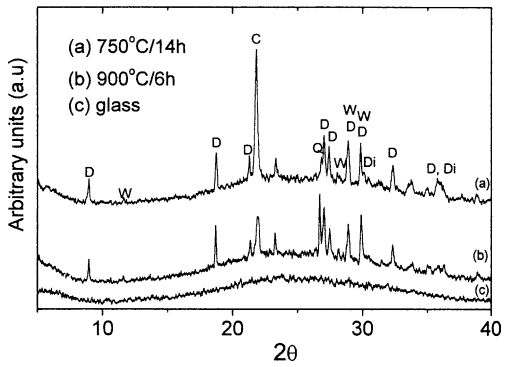

Fig. 7. X-ray patterns of the powdered sample heat-treated at: (a) 750 °C/15 h, (b) 900 °C/6 h and (c) glass spheres as received. D = devitrite, C = cristobalite, Q = quartz, W = wollastonite and Di = diopside.

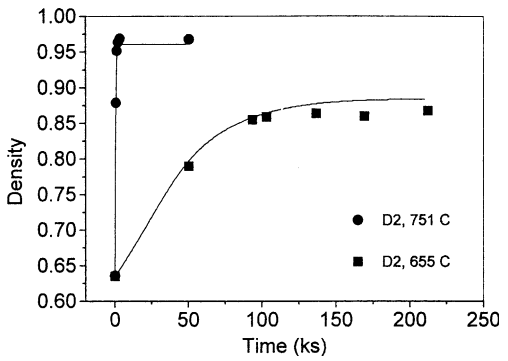

Fig. 9. Densification kinetics of D2 glass spheres at 751 and 655 °C. Line: calculated with the Clusters model. Solid symbols: measured.

density versus time curves for different temperatures. Isothermal sintering experiments were conducted simultaneously. Figs. 8 and 9 show the simulated and experimental densification curves at different temperatures for D1 and D2 glass beads.

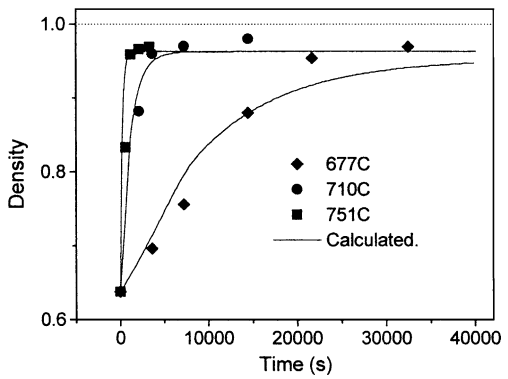

Fig. 8. Densification kinetics of D1 glass spheres at different temperatures. Lines: calculated with the Clusters model. Solid symbols: measured.

In order to further test the model, we performed sintering experiments with mixtures of as-received (mostly glassy) spheres with different fractions of spheres having fully pre-crystallized surfaces. These pre-crystallized spheres, with a 100% crystallized surface, were prepared by treatment at 600 °C for 3 days. At this temperature, surface

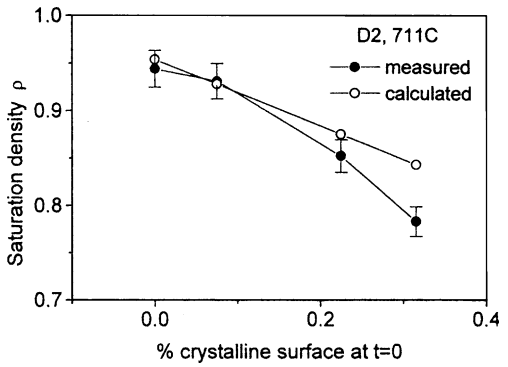

Fig. 10. Saturation density of sintered samples with different values of pre-crystallized surface. The calculated saturation densities also consider pre-existing foreign particles on the initial sphere and pore surfaces.

crystallization predominated over sintering, and slightly mixing the spheres during the beginning of the crystallization process sufficed to prevent the formation of necks.

Fig. 10 shows the calculated and measured final densities after sintering at 711 °C, for D2 samples including 0%, 6%, 22% and 30% of spheres having pre-crystallized surfaces. The theoretical and experimental results agree indicating that Eq. (10) can predict the decrease of saturation density with increased pre-crystallized surface fractions.

5. Discussion

Fig. 8 shows that, for the D1 beads, the measured densities are quite close to the values calculated with the Clusters model for a wide range of temperatures (677–751 °C), while Fig. 9 shows that the same observation is valid for the D2. The final (saturation) density in Fig. 8, predicted from calculations, depends on the sintering temperature. Higher temperatures lead to higher saturation densities; thus, higher temperatures favor sintering over crystallization. This fact is more marked in Fig. 9, where, after sintering D2 beads at 655 °C, the saturation density is only about 0.85. This demonstrates that sintering is hindered by crystallization and provides a stringent test for the Clusters model.

Crystallization is a determining factor that hinders further sintering at low temperatures (655 °C). Fig. 11 shows a SEM micrograph of D2 beads treated at 655 °C for 47 and 59 h. These are porous samples and details of the particles' boundaries reveal a good deal of surface crystallization.

The saturation density for samples heat-treated at 751 °C was 0.98, while our simulations predicted a slightly lower density of 0.96. This difference was also observed at other temperatures, except for D2, for which the final experimental density was lower than predicted. Although our calculations

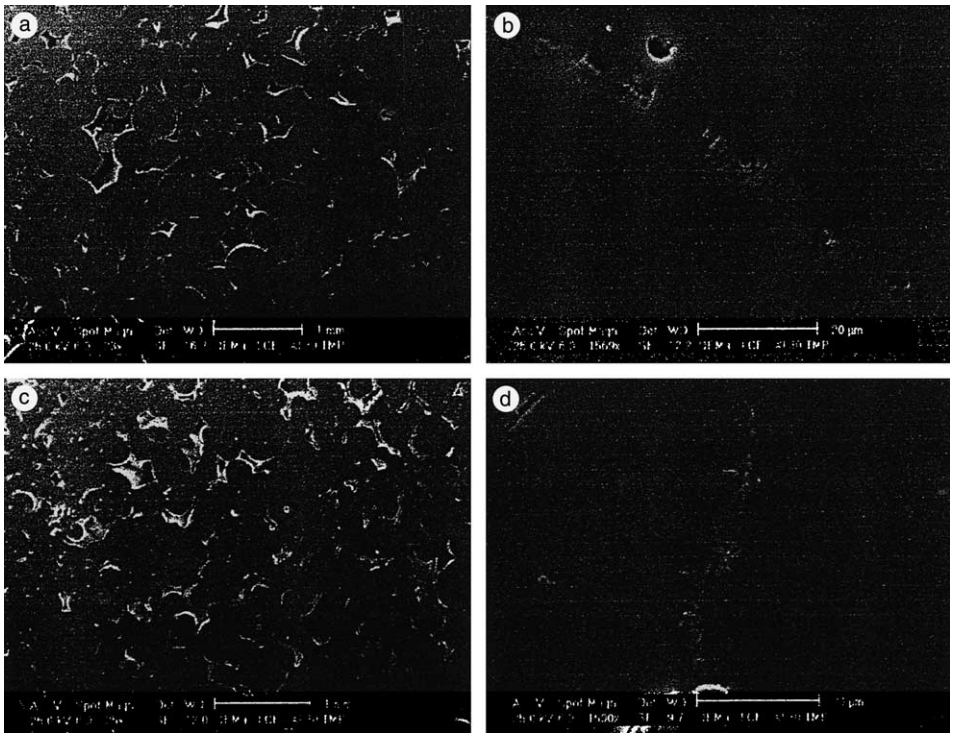

Fig. 11. SEM micrograph of the samples D2 heat-treated at 655 °C: (a) 47 h, (b) 47 h showing the particle boundary, (c) 59 h and (d) 59 h: showing the particle boundary.

considered the hindering effect of crystallization on sintering, we have evidence that at least other two factors can cause residual porosity: bubble formation due to the release of dissolved gas (which can be catalyzed by crystallization) and insoluble gases entrapped in the initial pores. For instance, water vapor and air (particularly N_2) have low solubility in silicate glasses. The final density also depends on the density of the new crystalline phases.

Fig. 12 shows micrographs of a D2 sample heat-treated at 673 °C for 29 h. Pores are visible at particle boundaries, as are crystals on their surface, suggesting that further heat-treatment could not completely densify this sample, since crystallization hinders sintering. The same phenomenon was observed in sample D2 heat-treated at 751 °C for 14 h (Fig. 13).

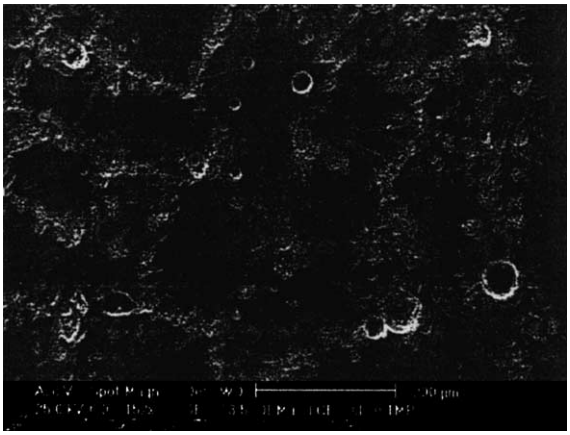

Fig. 13. SEM micrograph of a sample D2 heat-treated at 750 °C/14 h.

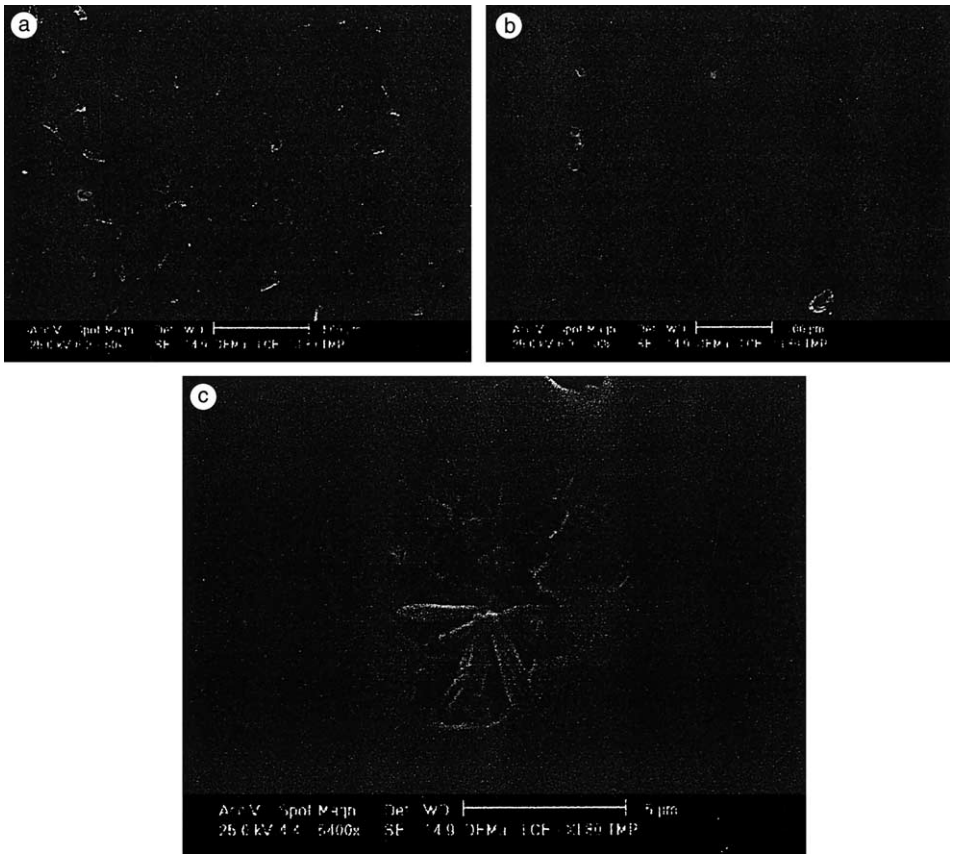

Fig. 12. SEM micrograph of D2 sample: (a) heat-treated at 673 °C/29 h, (b) the same sample showing bubbles in the particle boundaries and (c) showing crystallization in the pores.

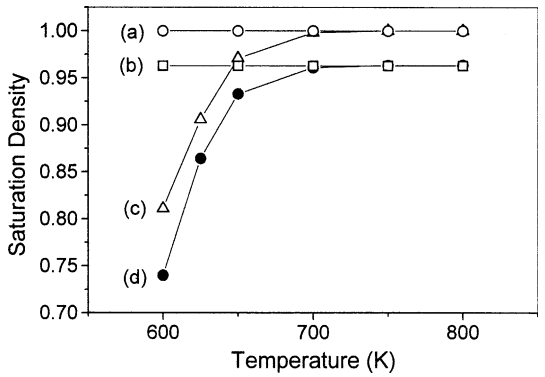

Fig. 14. Calculated saturation density versus sintering temperature for size distribution D1: (a) with glassy surface fraction = 1, without crystallization, (b) initial glass surface fraction = 0.9, without crystallization, (c) glassy surface fraction = 1 with concurrent crystallization, (d) initial glassy surface fraction = 0.9 with concurrent crystallization and pore surfaces with 10% of their area covered with foreign particles (actual studied system).

Fig. 14 displays the saturation density corresponding to isothermal sintering experiments of D1 sphere compacts. The curves were calculated with the present model for different imaginary situations: (a) with glassy surface fraction = 1, without crystallization, (b) initial glass surface fraction = 0.9, without crystallization, (c) glassy surface fraction = 1 with concurrent crystallization, (d) initial glassy surface fraction = 0.9 with concurrent crystallization (studied system). This analysis shows that pre-existing crystalline particles on the glass surface determine that saturation density will be lower than 1 if the pore surfaces are considered remainders of the original particle surfaces. Concurrent crystallization slows down the sintering kinetics, but at least in this case, does not prevent bodies from becoming fully sintered. In the absence of pre-existing crystals and of concurrent crystallization, saturation density = 1 can always be achieved, obviously disregarding particle degassing and other factors that prevent full densification.

For the present glass, temperatures exceeding 700 °C must be used to obtain maximum saturation density. In the case of non-isothermal sintering, a minimum heating rate is found in order to obtain maximum saturation density, Ref. [15].

Gaber et al. [16] showed that water, nitrogen and carbon oxides (CO, CO_2) surpass the sintering particles of soda-lime-silica glass with a dynamics that depends upon the particle size. Additionally, crystallization may induce gas release due to the different solubility of gases in the crystalline and vitreous phases. These gases may increase the porosity of the compact if they are generated during sintering. Fig. 12(a)–(c) show the microstructures of sintered D2 spheres. We suspect that the small bubbles appearing at the particles' boundaries are the result of degassing.

The results of several authors, as well as our own, show that is very difficult to achieve full densification. Even with an alumino borosilicate glass that barely crystallizes, Ref. [5], 2–3% of closed pores consistently remained in the glass, regardless of the sintering temperature.

In summary, taking into account all the complexities of this system, i.e., particle size distribution, defective particle packing, pre-existing surface crystals and four phases crystallizing concurrently with sintering, one can conclude that the congruence between calculated and experimental data is quite satisfactory.

6. Conclusions

The Clusters model was used to predict the isothermal sintering kinetics of polydispersed sphere compacts of soda-lime-silica glass undergoing concurrent crystallization. Since its sintering kinetics is quite complex due to the various crystalline phases that appear during crystallization and to the presence of foreign particles on its surface, this system was suitable to test the model's performance under stringent conditions. Overall, the experimental and calculated densification curves are similar for different size distributions, pre-crystallized surface fractions and temperatures, indicating the model's ability to include a series of measurable microstructural parameters and to account for different sintering temperatures and size distributions.

A common feature is that the density of the experimental compacts saturates at slightly different values than those predicted by the simulations.

When the maximum experimental densification is about 0.98, this saturation may be due to at least three factors: surface crystallization, entrapped insoluble gases in the initial pores and bubble formation owing to dissolved gas release (which can be catalyzed by crystallization). While the first cause – surface crystallization – is taken into account by the model equations, the other two are not.

Despite this drawback, the proposed algorithm provides a powerful simulation tool to design the densification of glass compacts undergoing surface crystallization and having every size distribution.

Acknowledgements

To CONICET and Comisión Nacional de Energía Atómica (Argentina) and to CNPq, Cyted, Pronex, and Fapesp (Brazil) for funding this research. Thanks are also due to Dr Eduardo B. Ferreira for his critical comments.

References

[1] E.M. Rabinovich, J. Mater. Sci. 20 (1985) 4259.
[2] J. Frenkel, J. Phys. (USSR) IX (5) (1945) 385.
[3] J.K Mackenzie, R. Shuttleworth, Proc. Phys. Soc. (London) Sect. B 62 (1949) 833.
[4] I. Gutzow, J. Schmelzer, The Vitreous State. Thermodynamics, Structure, Rheology and Crystallization, Springer, Berlin, 1995.
[5] M.O. Prado, E.D. Zanotto, R. Müller, J. Non-Cryst. Solids 279 (2001) 169.
[6] M.O. Prado, C. Fredericci, E.D. Zanotto, Chem. Phys. Glasses 5 (2002) 43.
[7] M.O. Prado, E.D. Zanotto, C. Fredericci, J. Mater. Res. 18 (6) (2003) 1347.
[8] E.A. Giess, J.P. Fletcher, L. Wynn Herron, J. Am. Ceram. Soc. 67 (8) (1984) 549.
[9] R. Müller, Glastech. Ber.Glass Sci. Technol. 67C (1994) 93.
[10] Y.M. Chiang, D.P. Birnie III, W.D. Kingery, in: Physical Ceramics. Principles for Ceramic Science and Engineering, John Wiley, New York, 1997, p. 392.
[11] R. Müller, M. Kirsch, H. Lorenz, XV Congress on Glass, Leningrad, vol. 3, 1989, p. 334.
[12] O.V. Mazurin, M.V. Streltsina, T.P. Shvaiko-Shvaikovskaya, V.K Leko, A.I. Priven, SciGlass TM 3.0, Universal Information System on Glass Properties. scivision@delphi.com, http://www.scivision.com.
[13] R. Müller, E.D. Zanotto, V.M. Fokin, J. Non-Cryst. Solids 274 (1–3) (2000) 208.
[14] J. Deubener, R. Brückner, H. Hessenkemper, Glastech. Ber. 65 (9) (1992) 256.
[15] M.O. Prado, C. Fredericci, E.D. Zanotto, J. Non-Cryst. Solids, this issue. doi:10.1016/j.jnoncrysol.2003.08.077.
[16] M. Gaber, R. Müller, W. Hölland, in: Proceedings of 6th International Otto Schott Colloquium, Jena, 1998 GlastechBer. Glass Sci. Technol. 71 C (1998) 353.